PCCP

Accepted Manuscript

ROYAL SOCIETY OF CHEMISTRY

www.rsc.org/pccp

Evidence for quantum effects in predissociation of methylamine isotopologues

Michael Epshtein, Alexander Portnov and Ilana Bar

The H product distributions obtained from methylamine isotopologues predissociation are extremely sensitive to the energy difference between the initially prepared vibrational states and the conical intersections and not only to the nature of the pre-excited nuclear motions.

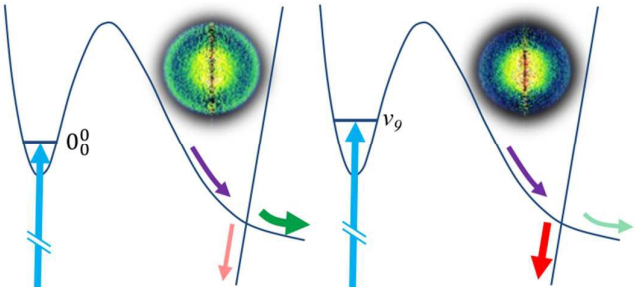

Evidence for quantum effects in predissociation of methylamine isotopologues†

Michael Epshtein, Alexander Portnov and Ilana Bar*

Non-adiabatic dynamics at conical intersections (CI) extensively affects the photostability of biomolecules by efficiently photoinducing decay routes that dissipate harmful excess ultraviolet energy. Here the predissociation of the model test molecules, methylamine (CH_3NH_2) and its partially deuterated isotopologue (CD_3NH_2), excited to different specific vibrational modes in the electronically excited state has been experimentally investigated. The H(D) photofragments were detected by two-color reduced-Doppler ion imaging, which allows measurement of their entire velocity distributions in each laser pulse. The fast and slow H products, resulting from N-H bond cleavage, obtained via different dissociation pathways, showed anomalous distributions for some vibronic states, as indicated by dynamic resonances in the product branching ratio and in the anisotropy parameters of the fast H photofragments. This vibronic-specific control is attributed to the sensitivity of the non-adiabatic dynamics to the energy difference between the initially prepared vibrational states and the energy of the CIs and not only to the distinctive pre-excited nuclear motions. The observations in the two isotopologues reveal uniquely detailed insight into the dynamics of state-specific control.

Submitted to *Phys. Chem. Chem. Phys*.

Department of Physics, Ben-Gurion University of the Negev, Beer-Sheva 84105, Israel.

* *E-mail:ibar@bgu.ac.il*.

† Electronic supplementary information (ESI) available. See DOI:

1 Introduction

Radiationless transitions play a key role in many aspects of different fields and became in the focus of studies that seek to understand and control the non-adiabatic dynamics at conical intersections (CIs).[1,2,3,4,5] These processes occur in electronically excited states, via nuclear motions that induce coupling between two (or more) close-lying adiabatic surfaces, which cross in at least a two-dimensional coordinate to generate a dynamic funnel. Indeed, radiationless transitions between electronic states of a molecule are of importance in a variety of processes, spanning from reactions as simple as the hydrogen-exchange reaction [6] to energy transfer in rhodopsin, involved in vision, [7] and to photostability of deoxyribonucleic acid (DNA) and ribonucleic acid (RNA) nucleotides, selected by evolution due to their faster internal conversion (IC) rates relative to those in bond scission.[2,5] As a consequence, the dynamic role of CIs in photodissociation of different compounds and especially in heteroatom containing aromatic species[8] that act as ultraviolet (UV) chromophores in DNA nucleobases and aromatic amino acids have been studied.

A very appealing system that received considerable interest over recent decades is the prototypical model of methylamine (CH_3NH_2) and its partially, or fully deuterated isotopologues, and particularly their photolysis following excitation to the first UV absorption band. This is due to their similarity with ammonia and relative simplicity, which made them liable to numerous experimental[9,10,11,12,13,14,15,16,17,18,19,20,21,22,23,24,25,26,27] and theoretical[28,29,30,31,32,33,34] studies. In particular, five dissociation channels have been discussed and identified,[9,10,27,28,29,30] including N-H, C-H and C-N bond cleavage that leads to $CH_3 + NH_2$, or $CH_4 + NH$, as well as H_2 elimination from both the amino and methyl groups. Nevertheless, most studies focused on H(D) photofragment

detection[11,12,15,18,19,20,21,22,23,24,25] resulting from N-H(D) and C-H(D) bond cleavage, where the former was found to be the dominant one.

The structured first UV absorption band of methylamine, in the 190 - 240 nm wavelength range, results from excitation of a nitrogen lone pair (*n*) electron into a bound 3*s* Rydberg orbital in the vertical Franck-Condon (FC) region, rapidly evolving into a dissociative n,σ^* orbital upon N-H bond extension.[29,30,31,32,33] This band, related to excitation between the $\tilde{A} \leftarrow \tilde{X}$ ($S_1 \leftarrow S_0$) potential energy surfaces (PESs), exhibits diffuse vibronic structure with vibrational progressions assigned to transitions involving excitation of amino wagging, ν_9, methyl rocking, ν_7, and their combinations.[13,14,15] The excitation to S_1 is also associated with a geometry change about the nitrogen atom from pyramidal to effectively planar.

An additional important feature of the spectra is that the bands of the isotopologues exhibit systematic blue shifts of the band origins upon H → D substitution.[15] Furthermore, the spectra of the isotopologues are characterized by different linewidths, corresponding to lifetimes of ~0.38 and ~8.8 ps at the CH_3NH_2 and CH_3ND_2 origins, respectively, decreasing somewhat and considerably for the former and the latter, respectively, at higher excitation energies. The short lifetime and the isotope effect indicate that tunneling through a barrier leads to predissociation and that the major channel is N–H, or N–D bond cleavage.[14] This was supported by time-dependent quantum wave-packet calculations of H and D atom tunneling in the respective molecules, showing it is faster in CH_3NH_2.[33] In addition, the promotion of CH_3NH_2 and of methylamine-d_3, CD_3NH_2, molecules to excited vibronic states in S_1, showed increased dissociation probabilities for H atoms as higher vibronic states were accessed.[24,25] Comparison of these results to those of an analytical model and to direct dynamical calculations, confirmed that the predissociation occurs by tunneling. The presence of a small barrier at short range on the S_1 PES, along the N−H

bond dissociation coordinate, as well as of a CI with the ground-state surface at larger bond extensions was also supported by *ab initio* calculation results.[28,29,30,31,32,33,34] The calculations also indicated that methylamine dissociates into hydrogen in the ground (^{2}S) state and CH_3NH in the first excited ($\tilde{A}$) state, or into ground state products H(^{2}S) + CH_3NH($\tilde{X}$), where the former channel results diabatically from S_0 and is energetically allowed only for excitation wavelengths of $\lambda < 203$ nm, and the latter from S_1.[30]

A more detailed view of the one-dimensional PE curves involved in the S_1 predissociation dynamics, as well as on the couplings and correlations with the dissociative states was obtained computationally by Kim and co-workers.[16] The S_1 state of methylamine was attributed to a predissociative state, obtained by vibronic coupling with the repulsive $n\sigma^*$ S_2 PES, along N–H bond elongation. They suggested that in the region of the S_1 well, the fast coupling occurs by tunneling through a reaction barrier, generated by the avoided crossing of the S_2 and S_1 surfaces. Following the dissociation process on the S_2 repulsive PES, an additional CI, between the S_2 and S_0 states, is encountered, finally leading to H + CH_3NH photofragments. Considering that the repulsive S_2 state correlates to ground state CH_3NH($\tilde{X}$) fragments and the S_0 correlates diabatically to excited CH_3NH ($\tilde{A}$), at the asymptotic limit, both products can be obtained.

It is interesting to note that most experimental studies that explored the N-H(D) fragmentation, lacked characterization of the starting quantum states of methylamines on the S_1 state, or the possibility to directly examine the state-selective predissociation dynamics at the CI. Actually, there was only a single experimental attempt that examined this aspect, by choosing several S_1 vibronic states, including the zero-point level and the ν_9 and $2\nu_9$ states in CH_3NH_2 and in CD_3ND_2 as well as the $3\nu_9$ state in the latter.[16] This study revealed a bimodal appearance of "fast" and "slow" H(D) photofragments, with branching ratios sensitive to the initial vibronic state for N–H bond dissociation in CH_3NH_2, but only

slightly affected the N–D cleavage in CD_3ND_2. In particular, it has been found that CH_3NH_2 containing one quantum of amino wagging leads to higher yield of slow H photoproducts. These findings bring up the intriguing questions of whether other specific vibrational modes in the electronically excited state of CH_3NH_2 could affect the branching ratios? Furthermore, could the relative yields of the two different channels change dramatically upon ν_9 excitation in CD_3NH_2?

In this work we represent the results of a unique and thorough study of the predissociation dynamics of CH_3NH_2 and of CD_3NH_2, initially excited to different specific vibrational modes in the S_1 electronically excited state. These two isotopologues, where the H in the methyl group was substituted by D, provide the opportunity to study the N-H bond cleavage in both compounds. Our approach, takes advantage of the frequency resolved two-color reduced-Doppler (TCRD) ion imaging[35] recently developed by us.[36] In this method two counterpropagating probe laser beams at close wavelengths are used, providing observation of the photofragments released with all velocities and therefore enhanced sensitivity in H(D) photofragment detection. This enabled to obtain insight into the predissociation dynamics of these species and by preparation of different initial vibrational states in S_1 control of the passage through the S_1/S_0 CIs (in frame of the simple picture of the involved states[29,30,31,32,33]), which altered the yield and the angular recoil anisotropy parameters, β, of the ensuing photofragments. Moreover, this work hints to the consequences of the energy difference between the initially prepared vibrational states and the energy of the CIs on the predissociation dynamics.

2 Methods

A detailed description of the experimental setup used in this study has been reported elsewhere.[36] Briefly, a home-built velocity map imaging (VMI) system,[37,38] containing a

source and a main detection chamber, differentially pumped and separated by a skimmer with a 0.08 cm diameter (dia.) aperture was used. The main advantage of VMI is that it simultaneously captures both the kinetic energies and the angular recoil trajectories (velocity vectors) of the original three-dimensional (3D) distributions of the ionized photofragments (Newton sphere) via collection of two-dimensional (2D) projections.

A pulsed molecular beam of methylamine (≥ 98 % purity, purchased from Sigma-Aldrich) or methylamine-d_3 (98 % purity, Cambridge Isotope Laboratories, Inc.) was prepared by supersonic expansion of a mixture of approximately 5 % of sample in argon carrier gas at a backing pressure of 1 bar. This mixture was delivered by a pulsed valve (General Valve, Series 9) with a 0.08 cm diameter orifice, positioned in the source chamber and pointing toward the detection plate. After passing through the skimmer located 3 cm downstream the nozzle orifice, the supersonic molecular beam entered into the VMI optics assembly located in the main chamber, consisting of three electrodes (repeller, extractor and ground). The operating pressures were maintained at 2 x 10^{-5} and 2 × 10^{-7} Torr in the source and main chambers, respectively.

The photolysis laser beam (227.50 – 239.95 nm) traversed the molecular beam at a right angle, while passing in the interaction region located halfway between the repeller and extractor electrodes. This beam was obtained from the doubled output of a tunable dye laser pumped by the third harmonic of a neodymium doped yttrium aluminum garnet (Nd:YAG) laser. The beam was vertically polarized, parallel to the detector surface, and was then focused with a 30 cm focal length (f.l.) lens into the interaction region. The typical output power for this pulsed laser beam was 40 μJ pulse^{-1}.

The H(D) atoms, released in the predissociation of methylamine or methylamine-d_3, were detected by TCRD (2 + 1) resonantly enhanced multiphoton ionization (REMPI) probing. In this technique, two counterpropagating laser beams, set at close wavelengths

of 243.12(243.05) and 243.15(243.09) nm, were used to effectively eliminate the Doppler broadening of the 2s ^{2}S ← 1s ^{2}S transition of the H(D) atoms. This enabled probing the entire velocity distributions of the H(D) photofragments in a single pulse without the need of scanning the beam across the Doppler width.

The first laser beam was obtained from the doubled output of the signal of an optical parametric oscillator (OPO), pumped by an injection-seeded Nd:YAG laser, while the second beam was produced by difference frequency mixing of the doubled output of an additional dye laser, pumped by the second harmonic of a third Nd:YAG laser, with the residual of the Nd:YAG fundamental. The temporal widths, full-width at half-maximum (FWHM) of the two laser beams were ~5 ns and the FWHM spectral width <0.2 and < 0.26 cm^{-1}, respectively. These beams with typical energies of 120 μJ pulse^{-1} were focused into the interaction region with 100 cm f.l. lenses, to temporally overlap and to minimize photofragments fly out. The probe beams were temporally delayed by ~4 ns relative to the photolysis beam (temporal and spectral FWHM ~5 ns and <0.2 cm^{-1}), which passed through a beam shutter (Thorlabs, SH05). This shutter was used for subtracting the contribution of ~243.1 nm photodissociation signal from the total signal.

The $H^+(D^+)$ ions were detected with a microchannel plate (MCP) coupled to a phosphor (P20) screen. Images were recorded with a charge-coupled device (CCD) camera (PCO, PixelFly 640 × 480 pixels) and accumulated over 25600 laser shots without additional processing. Mass selectivity was achieved by gating the voltage of the multichannel plate (MCP) ion detector. The molecular beam and the photolysis and probe lasers were pulsed at 10 Hz. The calibration of the H atom velocities was accomplished by recording O atom signals from the ~225 nm photolysis of O_2. All imaging measurements were made under velocity mapping conditions.

3 Results

The raw recorded 2D TCRD velocity map images of the H photofragments, following methylamine and methylamine-d_3 photolysis, via different specific vibrational modes [the 0_0^0 state, the ν_9 (NH_2 wag) and the ν_7 (CH_3 rock) fundamentals and the $2\nu_9$] (based on Ref. 15) in the first electronically excited states [panels (a), (b), (c) and (d)] and the corresponding central slices from the Abel inverted images[36] [panels (e), (f), (g) and (h)], which exhibit the 3D distributions, are shown in Figs. 1 and 2, respectively. In addition to the above, the $\nu_7 + \nu_9$, $3\nu_9$ and $\nu_7 + 2\nu_9$ states of both compounds, at higher excitation energies were also prepared, resulting in TCRD images very similar to those of $2\nu_9$ in the respective compounds. The specific vibrational modes for which the TCRD images were monitored appear in the H action spectra (taken from Ref. 24,25) that show the H photofragment yield obtained in predissociation of CH_3NH_2 (a) and CD_3NH_2 (b) molecules (see the electronic supplementary information (ESI†) online, Fig. S1).

Also shown are the consequent total kinetic energy distributions (green circles), exhibiting the total center of mass translational energy distributions. These distributions were obtained by integrating the 3D velocity distributions, Figs. 1(e)-1(h) and 2(e)-2(h), over the angular coordinates, while applying linear momentum conservation for the two photofragments. In addition, they were fitted by the red lines in Figs. 1(i)-1(l) and 2(i)-2(l), which result from contribution of two individual asymmetric components (blue lines) (see below).

It is clearly seen that the measured 2D TCRD images, Figs. 1(a)-1(d) and 2(a)-2(d), and even more so the center of the original 3D kinetic energy distribution slices, Figs. 1(e)-1(h) and 2(e)-2(h), exhibit inner features and sharper outer rings; reflected by the deconvoluted blue components [Figs. 1(i)-1(l) and 2(i)-2(l)]. These confirm the release of fast and slow H photofragments in predissociation of the N-H bond in CH_3NH_2 and

CD_3NH_2, via at least two distinctive channels. Previous studies[11,12,16] attributed the fast channel to molecules that directly pass via the CI to the ground-state asymptote, on the first encounter, and lead to H + $CH_3NH(\tilde{X})$, while the slow one to those that experienced IC when passing via the CI, from S_1 to the vibrationally "hot" S_0 state. It should be noted that the latter channel, obtained in CH_3NH_2 predissociation, includes a slight contribution from C-H bond cleavage.[11,12,24,25]

As a matter of fact, this is confirmed by the observed angular velocity distributions for the slow H atoms, resulting from CH_3NH_2 [Figs. 1(a)-1(d)] and CD_3NH_2 (Figs. 2(a)-2(d)] predissociation. These distributions are slightly anisotropic, with slight preference of parallel bond dissociation, relative to the photolyzing laser polarization. This behavior is most pronounced for the 0_0^0 state of CD_3NH_2, Fig. 2(a), which consists of H photofragments, solely resulting from N-H bond cleavage. These fragments possess a higher anisotropicity than those obtained in CH_3NH_2 predissociation, Fig. 1(a), which also includes H atoms resulting from C-H bond cleavage. Indeed, it can be seen that the measured TCRD image of the D photofragment, obtained following excitation to the 0_0^0 state of CD_3NH_2 is isotropic (see the electronic supplementary information (ESI†) online, Fig. S2). If this contribution would be taken in account, a more isotropic behavior for the slow channel would be expected, like in CH_3NH_2. It turns out that the angular velocity distributions of the D atoms, ensuing following pre-excitation to higher vibronic states behave similarly, exhibiting isotropic distributions.

As for the angular velocity distributions of the fast H atoms, it seems that they strongly depend on the initial accessed vibrational modes, showing favored bond breaking in the perpendicular direction for the modes ν_9 in CH_3NH_2, Fig. 1(f), and ν_9 and ν_7 in CD_3NH_2, Figs. 2(f) and 2(g), and somewhat more isotropic behavior for shorter wavelengths. Furthermore, examination of the velocity distributions, displayed in Figs. 1

and 2 [(i), (j), (k) and (l)], shows that the branching ratios between the slow and fast H photofragments, which are obtained from the integrated components are also mode dependent. It is obvious that the branching ratios are sensitive to the individual asymmetric components that were used to fit the fragments distributions, however, due to reasonable quality of the fits in Figs. 1(i)-1(l) and 2(i)-2(l) it seems that the derived values are reliable. Therefore, although the fast hydrogen atoms are dominant for most modes, it appears that for excitation energies corresponding to the ν_9 in CH_3NH_2, Fig. 1(f), and ν_9 and ν_7 in CD_3NH_2, Figs. 2(f) and 2(g), a notable increase in slow H atoms occurs.

These observations are even more obvious from the data shown in Figs. 3(a) and 3(b) that display the H branching ratios and the β parameters,[39,40] as a function of excitation energy. In particular, it can be clearly seen that the ν_9 state in CH_3NH_2 and the ν_7 and ν_9 states in CD_3NH_2 exhibit a striking increase in the branching ratios, due to the significant contribution of the slow H photofragments in the dissociation, namely preferred IC, via the CI, to the vibrationally hot S_0 state. In fact, the branching ratios between the slow and fast H photofragments are quite constant, around 0.4 and 0.3 for CH_3NH_2 and CD_3NH_2, respectively, but they unexpectedly increase to 1.0 and ~ 0.43 at these unique energetic points. For CH_3NH_2, a similar effect was also observed by Kim and co-workers,[16] although with a different ratio.

It is interesting to note that this rise in branching ratio exactly matches the sudden increase in β parameters for fast H atoms. Consequently, these unique energetic points lead to a dramatic rise in the relative yield of the slow H photofragments and in the anisotropy of the fast ones, and are believed to indicate presence of dynamic resonances (see below).

As implied from inspection of Figs. 1(e)-1(h) and 2(e)-2(h) the β parameters, which represent the vector properties of the transition dipole moments with respect to the bond-

dissociation axis, are consistently negative for the fast H photofragments, involving little preference for perpendicular bond dissociation compared to the photodissociationg laser polarization. They reach values around -0.1 to -0.25 for all the initially excited vibronic states, rising to about -0.7 for ν_9 in CH_3NH_2 and -0.5 for ν_9 and ν_7 in CD_3NH_2, respectively. In contrast to this behavior, the slow H atoms do not exhibit any resonances in the β parameters, Figs. 3(a) and 3(b), but rather show evidence for slight preference for parallel bond dissociation relative to the photolysis laser polarization. The retrieved values are about +0.1 for all the initially prepared modes in CH_3NH_2 and around +0.35 for the 0_0^0 state of CD_3NH_2, gradually decreasing to +0.1 as higher vibronic states are accessed. As mentioned above, the anisotropy parameters of CD_3NH_2 are somewhat "purer", since they include only H photofragments resulting from N-H bond cleavage.

4 Discussion

These findings offer deep insight into the origin of the N-H dissociation dynamics of methylamine and its isotopologue. Although it is obvious that understanding the dynamics requires multidimensional PESs, considering the simple diagram of the PESs along the N–H bond dissociation coordinate can also be very helpful. As can be seen from the schematic drawing of the PESs, Fig. 4(a), the key factors affecting the dynamics, reminiscent of the behavior observed and rationalized in ammonia,[11,12] are the tunneling of the dissociating molecules, through the small barrier in the N–H stretch coordinate,[14,24,25,29,30,31,33] and the subsequent passage through the S_1/S_0 CI at larger $R_{N\text{-}H}$.[29,30,31,32,33,34]

As for tunneling, it is already well known that the isotopologues containing the ND_2 moiety exhibit narrower linewidths in the first few vibronic bands, than those containing the NH_2 group.[15] For instance, a remarkable difference between the lifetimes of

the vibronic ground state in CH_3ND_2 (8.8 ± 0.7 ps) and CH_3NH_2 (0.38 ± 0.03 ps) was found. For higher vibronic states of CH_3NH_2 the lifetime varies only slightly upon increase of the vibrational energy, while for CH_3ND_2 it decreases to < 0.7 ps for the $2\nu_7$ vibrational state.[14] It is worth noting that the huge difference in lifetimes for the zero-point level was considered to be persuasive evidence of tunneling between the initially excited Rydberg state and the dissociative state.

Since H to D substitution on the methyl group is not expected to alter the tunneling rate of the H departing from the NH_2 moiety, it is likely that the lifetimes of the vibronic states in CD_3NH_2 resemble those in the CH_3NH_2 molecule. In addition, the H tunneling probabilities from the excited vibronic states, vs excitation energy were found to show a similar trend, i.e., smooth increase as higher initial vibronic states are accessed.[24,25] Therefore, this behavior, where no sudden change in lifetimes, or in transition probabilities occurred, seems to be an indication that the passage through the barrier does not play a unique role in the state-specific predissociation dynamics of CH_3NH_2 and CD_3NH_2. It is rather likely that the CIs between the dissociative and ground electronic states are responsible for the non-adiabatic dynamics, leading to bimodal distributions of the H photofragments, during N-H bond breaking and to the resonances in the branching ratio and in the β parameters of fast H atoms with respect to initially excited specific modes in the two molecules**.**

Based on the acquired velocities, it is reasonable to assume that the fast H atoms mainly evolve from molecules that start to dissociate upon N-H bond extension, while passing through the CI and eventually accessing the ground-state asymptote. However, it could be possible that the molecules fail to pass the CI on first traversal and since the first electronically excited $CH_3NH(\tilde{A})$ is not energetically accessible at the excitation energies used here,[29] the molecules are expected to be bounced off the inclined potential wall and

revisit the CI afterward. On that occasion, the molecules will either traverse the CI or miss it and pass it even later. The passage of molecules via the CI can take place toward the asymptote, or non-adiabatically to the hot ground-state that later dissociates, following energy redistribution among the vibrational states. This implies that the partner photofragments, $CH_3NH(\tilde{X})$ and $CD_3NH(\tilde{X})$, acquire more of the available energy, leading to slower H photofragments.

This picture is supported by the retrieved β parameters. While the previous study on initially excited vibronic states of CH_3NH_2,[16] reported a variation in the recoil β parameters as a function of translational energy, with values from +0.2 to +0.8, with tendency of higher values for the fast H photofragments; our study, shows positive and negative β values for H photofragments with low and high recoil energies, respectively, released in CH_3NH_2 and CD_3NH_2 predissociation. The discrepancy between the results could be due to the different employed imaging methods, i.e., VMI[16] and TCRD. However, since the TCRD imaging, used here, allows measurement of the entire velocity distributions in each laser pulse, leading to higher signal to noise ratio, it is expected to lead to more reliable β parameters.

Actually, the β parameters depend on the identity of the involved states and the transition geometry. Considering that $\boldsymbol{\mu}$ lies perpendicular to the NH_2 moiety, like in ammonia, it seems reasonable to assume that the dissociating molecules approach the CI with (essentially) planar geometries and pass to the ground-state surface asymptote. In this case, the H and ground state radical photofragments separate in the plane perpendicular to $\boldsymbol{\mu}$ and the former show negative β. On the other hand, molecules that approach later the CI probably possess non-planar geometries, so that the H fragments are thrown out of the original plane of the excited state molecule, leading to positive βs.

The negative and positive βs of the H photofragments, resulting from the predissociation of most initially prepared vibronic states, are quite low, but they show remarkable increase for fast H photofragments, resulting from the pre-excited ν_9 state of CH_3NH_2, Fig. 3(a), and ν_9 and ν_7 of CD_3NH_2, Fig. 3(b). This might be an indication that the dissociation from these states occurs promptly, within the molecular rotation period. The higher slow/fast H photofragments branching ratios, Figs. 3(a) and 3(b), allude to the higher probability for crossing non-adiabatically through the CI to the ground-state for these initially prepared states. Therefore, it seems that for these molecules, the contribution of fast photofragments that pass the CI to the ground-state asymptote at a later encounter is minimized, leading to significantly higher β parameters.

Accordingly, it is obvious that ultrafast dynamics contributes significantly to the high energy portions of the total kinetic energy spectrum, but it turns out that it also plays a role in the low portion. Of particular note are the β parameters of the slow H photofragments, ensuing in CD_3NH_2 predissociation, starting at +0.35 for the 0_0^0 state, and gradually decreasing for other initially prepared states at higher energies. This slight effect might be a result of the energetic proximity of the 0_0^0 state to the CI, which leads to molecules that slide on the PES, along the N–H coordinate, and pass through the CI to S_0, without being trapped for too long in the upper cone of the CI. The more isotropic velocity distributions, obtained as a result of preparation of higher vibronic states of the H photofragments, imply that the molecules pass the CI at a later encounter. In this case they are trapped for longer times in the upper cone of the CI, passing through it later and tending toward isotropic behavior.

Finally, of particular interest is the observation of the dynamic resonances, which are not of themselves new phenomena. For example in the photodissociation of thioanisole,[41,42] it was suggested that populating the S–CH_3 stretch mode, ν_{7a}, in the $^1\pi\pi^*$

state, leads to a marked change in the electronic branching in the C_6H_5S radical products. In these experiments, a very sharp resonance was observed at 722 cm^{-1} and it was suggested that this band allows direct transition from the S_0 to the S_1/S_2 superposition state that is close to the CI between these two states.

The interesting experimental observations of anomalous branching ratios, correlating to the β parameters of ν_9 in CH_3NH_2, Fig. 3(a), and ν_9 and ν_7 in CD_3NH_2, Fig. 3(b), (both of a' symmetry) and particularly the comparison between the effective initial modes in the two compounds may add a clue regarding the relation between the initially excited vibronic states and the dynamics at the CIs.

Both isotopologues, CH_3NH_2 and CD_3NH_2, comprise the NH_2 moiety and therefore it is expected that their PESs, along the N–H bond dissociation coordinate, would be quite similar. Nevertheless, their zero-point energies (ZPE) in the S_0 and S_1 states differ, being somewhat lower for CD_3NH_2.[15] These differences lead to a change in the energies of the band origins, T_o, where in CD_3NH_2 it is ~130 cm^{-1} above that in CH_3NH_2. Thus by considering the expanded schematic diagrams of the CH_3NH_2, Figs. 4(b), and of CD_3NH_2, Fig. 4(c), PESs, where the latter was shifted, accordingly, toward lower energy, it is reasonable to assume that this also applies to its ZPE and to its CI. At this instance, the initially prepared vibrational state in CH_3NH_2, the NH_2 wagging (ν_9) is allocated just between the ν_9 and the CH_3 rock, ν_7, of CD_3NH_2, relative to the CI. The sharper resonance in the branching ratio of the H photofragments and in the β parameter of the fast channel, obtained via preparation of ν_9 in CH_3NH_2, than those attained by excitation of ν_9 and ν_7 in CD_3NH_2, allude to the important role played by the energy difference between the initially prepared vibrational states and the CIs.

The H product distributions reflect the outcome of the predissociation of both molecules, when initiated at distinctive initially excited states, and are very sensitive to the

dynamics in the CI vicinity. Particularly, the dynamical resonances have the most pronounced effect and they guide the dynamics at the CIs. Considering that the initially prepared wavepackets start at particular energies, it is very reasonable to assume that they reach the CI with momentum that leads to their splitting. Therefore, a part of it continues toward the asymptote of the ground state, leading to the fast photofragments, and the rest climbs on the inclined potential wall, where it is recoiled. This can trap a part of the dissociating flux in the upper cone, which may lead to quantum interferences, affecting the bifurcation dynamics and the passage efficiency through the S_1/S_0 CIs (see Fig. 4). In particular, the dynamical resonances guide the passage of molecules, through the CI, to the hot ground state, leading to enhanced release of slow H photofragments. The observed results show that the dynamics is extremely sensitive to the energy difference between the initially prepared vibrational states and the CIs in the two molecules and not only to the unique nuclear motion promoting the predissociation.

In front of yet challenging calculations, it is obvious that predissociation studies, initiated by accessing different specific vibrational modes in the electronically excited states allow dynamics predesign, exerting control on the ensuing photoproducts. In particular, the trapping of the flux in the upper CI cone is affected by the energetic position of the initially excited vibrational states, relative to the CI. This work paves the way for probing dynamical resonances in additional molecular systems and for revealing their effect on branching ratios, the β parameters and how they guide the dynamics.

Acknowledgments

The support of this research by the Israel Science Foundation (ISF) under Grant No. 1001/09 is gratefully acknowledged.

References and Notes

1 D. R. Yarkony, *Rev. Mod. Phys*. 1996**, 68**, 985-1013.

2 A. L. Sobolewski and W. Domcke, *Europhys. News* 2006, **37,** 20-23.

3 S. Nanbu, T. Ishida and H. Nakamura, *Chem. Sci.* 2010, **1**, 663-674.

4 P. S. Christopher, M. Shapiro and P. Brumer, *J. Chem. Phys*. 2005, **123**, 064313-064319.

5 T. I. Sølling,T. S. Kuhlman, A. B. Stephansen, L. B. Klein and K. B. Møller, *Chem. Phys. Chem*. 2014, **15**, 249-259.

6 J.C. Juanes-Marcos, S.C. Althorpe and E. Wrede, *Science* 2005, **309**, 1227-1230.

7 R. W. Schoenlein, L. A. Peteanu, R. A. Mathies and C. V. Shank, *Science* 1991, **254**, 412-415.

8 M. N. R. Ashfold, B. Cronin, A. L. Devine, R. N. Dixon and M. G. D. Nix, *Science* 2006, **312**, 1637-1640.

9 J. V. Michael and W. A. Noyes, *J. Am. Chem. Soc*. 1963, **85**, 1228-1233.

10 G. C. G. Waschewsky, D. C. Kitchen, P. W. Browning and L. J. Butler, *J. Phys. Chem*. 1995, **99**, 2635-2645.

11 C. L. Reed, M. Kono, and M. N. R. Ashfold, *J. Chem. Soc. Faraday Trans*. 1996, **92**, 4897-4904.

12 M. N. R. Ashfold, R. N. Dixon, M. Kono, D. H. Mordaunt and C. L. Reed, *Philos. Trans. R. Soc. London, Ser. A* 1997, **355**, 1659-1676.

13 S. J. Beak, K.-W. Choi, Y. S. Choi and S. K. Kim, *J. Chem. Phys*. 2002, **117**, 10057-10060.

14 S. J. Beak, K.-W. Choi, Y. S. Choi and S. K. Kim, *J. Chem. Phys*. 2003, **118**, 11026-11039.

15 M. H. Park, K. -W. Choi, Y. S. Choi and S. K. Kim, *J. Chem. Phys.* 2006, **125**, 084311.

16 D. S. Ahn, J. Lee, J. -M. Choi, K. –S. Lee, S. J. Baek, K. Lee, K. -K. Baeck and S. K. Kim, *J. Chem. Phys*. 2008, **128**, 224305.

17 D. S. Ahn, J. Lee, Y. C. Park, Y. S. Lee and S. K. Kim, *J. Chem. Phys.* 2012, **136**, 024306.

18 A. Golan, S. Rosenwaks and I. Bar, *J. Chem. Phys*. 2006, **125**, 151103.

19 A. Golan, S. Rosenwaks, and I. Bar, *Isr. J. Chem*. 2007, **47**, 11-16.

20 A. Golan, A. Portnov, S. Rosenwaks and I. Bar, *Phys. Scr.* 2007, **76**, C79-C83.

21 R. Marom, U. Zecharia, S. Rosenwaks and I. Bar, *J. Chem. Phys*. 2008, **128**, 154319.

22 R. Marom, U. Zecharia, S. Rosenwaks and I. Bar, *Mol. Phys.* 2008, **106**, 213-222.

23 R. Marom, T. Weiss, S. Rosenwaks and I. Bar, *J. Chem. Phys*. 2009, **130**, 164312-164317.

24 R. Marom, C. Levi, T. Weiss, S. Rosenwaks, Y. Zeiri, R. Kosloff and I. Bar, *J. Phys. Chem. A* 2010, **114**, 9623-9627.

25 R. Marom, T. Weiss, S. Rosenwaks and I. Bar, *J. Chem. Phys*. 2010, **132**, 244310.

26 J. O. Thomas, K. E. Lower and C. Murray, *J. Phys. Chem*. *Lett.* 2012, **3**, 1341-1345.

27 J. O. Thomas, K. E. Lower and C. Murray, *J. Phys. Chem. A* 2014, **118**, 9844-9852 ().

28 E. Kassab, J. T. Gleghorn and E. M. Evleth, *J. Am. Chem. Soc.* 1983, **105**, 1746-1753.

29 K. M. Dunn and K. Morokuma, *J. Phys. Chem*. 1996**, 100**, 123-129.

30 H. Xiao, S. Maeda and K. Morokuma, *J. Phys. Chem. A* 2013**, 117**, 5757-5764.

31 C. Levi, G. J. Halász, Á. Vibók, I. Bar, Y. Zeiri, R. Kosloff and M. Baer, *J. Chem. Phys.* 2008, **128**, 244302.

32 C. Levi, G. J. Halász, Á. Vibók, I. Bar, Y. Zeiri, R. Kosloff, M. Baer, *Int. J. Quantum Chem.* 2009, **109**, 2482-2489.

33 C. Levi, R. Kosloff, Y. Zeiri and I. Bar, *J. Chem. Phys.* 2009, **131**, 064302.

34 C. Levi, G. J. Halász, Á. Vibók, I. Bar, Y. Zeiri, R. Kosloff and M. Baer, *J. Phys. Chem. A* 2011, **113**, 6756-6762.

35 C. Huang, W. Li, M. Kim and A. G. Suits, *J. Chem. Phys*. 2006, **125**, 121101.

36 M. Epshtein, A. Portnov, R. Kupfer, S. Rosenwaks and I. Bar, *J. Chem. Phys*. 2013,**139**, 184201; and references therein.

37 D. W. Chandler, and P. L. Houston, *J. Chem. Phys*. 1987, **87**, 1445-1447.

38 A. T. J. B. Eppink and D. H. Parker, *Rev. Sci. Instrum*. 1997, **68**, 3477-3484.

39 The respective branching ratios and angular recoil anisotropy parameters, β, were obtained by integrating the two channels fit components in Figs. 1(i) - (l) and 2(i) - (l) and by integrating the 3D velocity maps in Figs. 1(e) – (h) and 2(e) – (h) over the radii and fitting them to the equation for normalized angular distribution of photofragments,[40] namely $I(\theta) = (4\pi)^{-1}[1 + \beta P_2(\cos\theta)]$, while averaging approximately over the half height of the fit components. θ is the angle between **v** and the electric vector of the dissociating light, $P_2(\cos\theta)$ is the second Legendre polynomial, and β is a parameter that describes the degree of anisotropy ($-1 \le \beta \le 2$).

40 R. J. Van Brunt and R. N. Zare, *J. Chem. Phys*. 1968, **48**, 4304-4308.

41. J. S. Lim and S. K. Kim, *Nature Chem*. 2013, **2**, 627-632.

42. G. M. Roberts, D. J. Hadden, L. T. Bergendahl, A. M. Wenge, S. J. Harris, T. N. V. Karsili, M. N. R. Ashfold, M. J. Paterson and V. G. Stavros, *Chem. Sci*. 2013, **4**, 993-1001.

Figure Captions

Fig. 1. Measured two-color reduced-Doppler velocity map images of the H photofragments (unsymmetrized), following (a) 239.95, (b) 236.35, (c) 234.30 and (d) 232.70 nm photolysis of methylamine, corresponding to excitation of the 0_0^0 state, the ν_9 (NH_2 wag) and the ν_7 (CH_3 rock) fundamentals and the $2\nu_9$. The respective Abel inverted images in (e), (f), (g) and (h) and the measured total kinetic energy distributions (green circles) in (i), (j), (k) and (l), fitted by the red lines, represent the contributions of fast and slow atoms

(blue lines). The arrow in the right corner indicates the vertical polarization of the photolysis laser.

Fig. 2. Measured two-color reduced-Doppler velocity map images of the H photofragments (unsymmetrized), following (a) 239.35, (b) 236.15, (c) 234.80 and (d) 232.50 nm photolysis of methylamine-d_3, corresponding to excitation of the 0_0^0 state, the ν_9 (NH_2 wagging) and the ν_7 (CH_3 rock) fundamentals and the $2\nu_9$. The respective Abel inverted images in (e), (f), (g) and (h) and the measured total kinetic energy distributions (green circles) in (i), (j), (k) and (l), fitted by the red lines, represent the contributions of fast and slow atoms (blue lines). The arrow in the right corner indicates the vertical polarization of the photolysis laser.

Fig. 3. The branching ratios and β anisotropy parameters obtained for (a) CH_3NH_2 and (b) CD_3NH_2. Blue and red circles represent the ratios of slow to fast H photofragments as a function of the exciting energy, green and purple triangles and cyan and orange squares represent the β parameters of the slow and fast H atoms, respectively.

Fig. 4. (a) Simple diagram of the S_0 and S_1 electronic potential energy surfaces of methylamine, with respect to the N-H bond. Expanded portions of the conical intersection regions and of the S_1 surfaces in (b) CH_3NH_2 and (c) CD_3NH_2, where the band origin in CD_3NH_2 is shifted by ~130 cm^{-1} relative to that of CH_3NH_2. This shift positions the NH_2 wagging, ν_9, of CH_3NH_2 just between the ν_9 and the CH_3 rock, ν_7, of CD_3NH_2. The encircled regions signify the CIs.